Journal of Inflammation Research

Dovepress
Taylor & Francis Group

Open Access Full Text Article

ORIGINAL RESEARCH

Effects of Emodin on Lung Inflammation and Intestinal Microbes in Chronic Obstructive Pulmonary Disease

Jiaqian Xue*, Qingwei Zhou*

Respiratory Department of the First Affiliated Hospital of Henan University of Chinese Medicine, Zhengzhou, 450000, People's Republic of China

*These authors contributed equally to this work

Correspondence: Jiaqian Xue, Email 13608675981@163.com

Introduction: The impact of COPD on human health is enormous. Emodin, which has anti-inflammatory, anti-cancer, spasmolysis, and laxative effects, has not been systematically investigated within a study with regard to the treatment of COPD.

Methods: In this study, we conducted Experiment 1 to evaluate the effects of emodin on COPD. Emodin was purchased from Shanghai Yuanye Biotechnology Co. Ltd. (batch number: T17A10F95418). Pathological changes in lung tissue and the average lung lining interval were used to evaluate the severity of emphysema. Inflammatory cell counts in alveolar lavage fluid and the ratio of neutrophils and lymphocytes were used to observe the level of inflammation. The level of HMGB1-RAGE expression was determined via PCR. Moreover, we compared changes in the metabolites of the intestinal microbial community following an intervention with emodin. In Experiment 2, we observed the effect of fecal on the inflammatory response in COPD mice. A mouse dual intervention model was established using flora depletion and COPD modeling. We evaluated the general health of the model mice, specific pathological changes in lung tissue, the average lung lining interval, inflammatory cell counts within the alveolar lavage fluid, and HMGB1-RAGE pathway expression.

Results: Our results demonstrated that emodin statistically significantly improved lung tissue inflammation in COPD mice, and that butanoic acid was the main differential metabolite in intestinal bacteria. Transplanting the feces of the emodin group mice in Experiment 1 to the model mice evaluated in Experiment 2 reduced the infiltration of inflammatory cells and down-regulated the HMGB1-RAGE inflammation pathway.

Conclusion: Our findings provide important information for guiding future research directions.

Keywords: chronic obstructive pulmonary disease, emodin, neutrophils, gut microbiome, short-chain fatty acids, fecal microbiota transplantation

Introduction

Chronic obstructive pulmonary disease (COPD) is a devastating and high-incidence lung disease,[1] the global burden of COPD is still increasing. The latest global epidemiological research shows that, COPD is one of the top ten causes of disability in the elderly population over 65 years of age.[2]

The established risk factors for COPD include smoking, exposure to harmful particles in the ambient environment, bacterial and viral infections, and a family (ie, genetic) history. These factors act on the lungs to cause chronic inflammation, which further leads to airway stenosis and damage to the lung tissue structure, and finally causes the patient to present with clinical manifestations such as chronic cough, sputum production, chest tightness, and wheezing.

Rheum palmatum L. is one of the most commonly used Chinese medicines due to its observed effects on the lungs and large intestines. Early network pharmacology studies have shown that *Rheum palmatum L*. may treat COPD by regulating inflammation pathways.[3] Emodin is one of the main components of *Rheum palmatum L*. Studies have shown that emodin can reduce the inflammatory reaction of lung tissue caused by LPS by inhibiting the focal death pathway,[4] promoting the apoptosis of neutrophils and down-regulating the expression of reactive oxygen species.[5] At the same time, it also shows obvious anti-inflammatory effect in various animal models of inflammation.[6] However, there are few studies on the

Received: 4 April 2025
Accepted: 9 July 2025
Published: 23 July 2025

Graphical Abstract

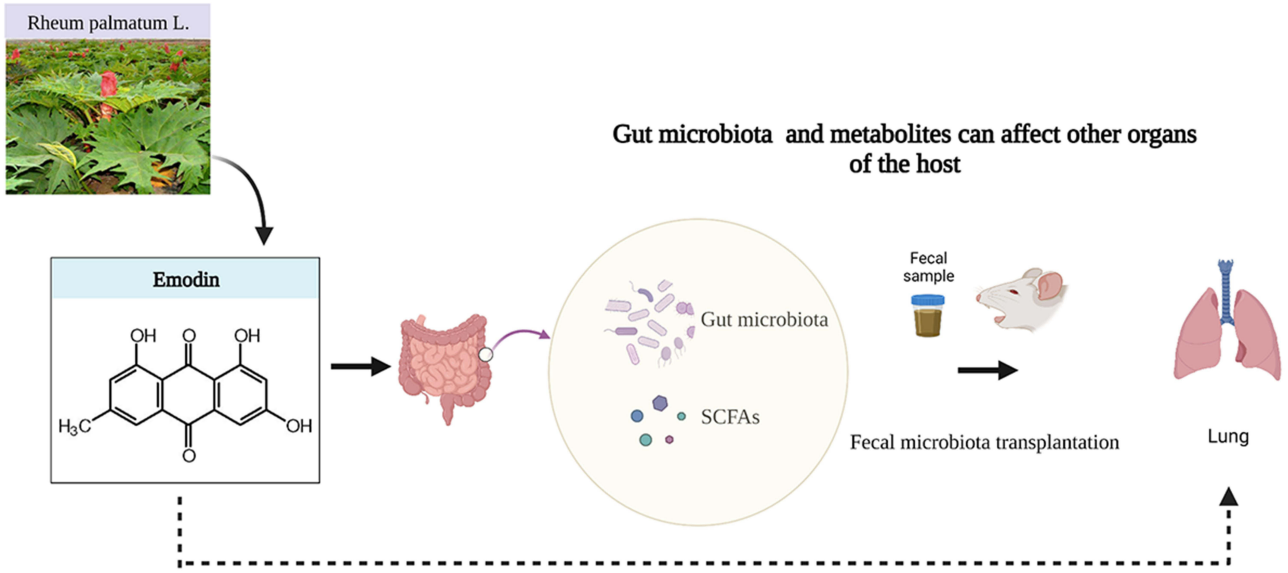

effects of emodin on lung and intestine. This study evaluated the gut-lung axis in order to evaluate the effects of emodin on the metabolites of intestinal flora as well as with regard to RAGE (receptor for advanced glycation end products)-associated pathways and inflammatory responses in lung tissues. Moreover, we aimed to further improve the state of knowledge regarding the "gut-lung" axis mechanism, to evaluate evidence with regard to the traditional Chinese medicine theory that "the lung and the large intestine are external and internal", and to promote efforts towards the prevention and treatment of COPD.

Materials and Methods

Experimental Design

Experiment 1: Emodin was purchased from Shanghai Yuanye Biotechnology Co., Ltd. (batch number: T17A10F95418). Mice were divided into a control group, a model group, and an emodin group (emodin, 40mg/kg, administered via gavage), with five mice in each group. From the 5th week onwards, each group was given drugs by gavage treatment (once a day at 0.2 mL) until the end of the 8th week of the experiment. This experiment was conducted in order to observe the effects of emodin intervention on COPD as well as the composition of the intestinal flora in mouse models.

Experiment 2: The mice were divided into a control group, a double model group (bacterial depletion + COPD modeling), and a transplanted emodin group (bacterial depletion + COPD modeling + emodin + mouse fecal bacteria transplantation), with five mice in each group. This experiment was conducted in order to study the effects of FMT (fecal microbiota transplantation) on inflammation associated with COPD.

COPD Mouse Model

SPF-grade (ie specific-pathogen-free) C57BL/6 male mice (age, 6–8 weeks; weight, 18–22g) were purchased from the Shanghai Laboratory Animal Center (certificate number: 20170005021681). The mice were kept at a constant temperature of 20±2°C and were housed in a 12-hour light/12-hour night alternating light pattern cycle. Smoke exposure combined with a lipopolysaccharide (LPS) tracheal drip method were used to establish the disease mouse model.[7]

Except for the control group, all mice were anesthetized by intraperitoneal injection with 1% pentobarbital on day 1, day 14, and day 28, which was converted to a dose of 50 mg/kg and slowly injected along with LPS solution at a concentration of 10mg/50μL (Sigma, USA). Each mouse was injected with 50μL of this solution.

Smoking was not allowed on the day of the surgery. Starting on the second day after LPS instillation, each group of mice were placed in a specialized COPD model-inducing smoked and poisoned device with the smoke concentration set to 5% and were "smoked" twice a day, burning eight cigarettes each time in a session lasting for 30 minutes. The interval between the two smoking exposures was 2–3 hours. "Smoking" was continued for eight weeks. Meanwhile, the normal mice breathed normal air.

All animal experiments were approved by the Experimental Animal Ethics Committee of the Henan University of Chinese Medicine (NO. LAC20230523[01]) and complied with the requirements of the National Academic Research Council guidelines with regard to the feeding, management, and use of laboratory animals (eight edition). This study was conducted in compliance with all relevant national and international guidelines on humane animal care and experimentation, including the ARRIVE guidelines.

Bacterial Depletion

Ampicillin (1g/L), neomycin (1g/L), metronidazole (1g/L), and vancomycin (500 mg/L) were dissolved into the drinking water of the evaluated mice in order to form a mixture of antibiotics. The mice were allowed to drink this water freely for five days and were then given normal drinking water for three days in order to create a bacterial depletion mouse model.

Fecal Microbiota Transplantation

Approximately 100 mg of mouse feces were taken from each group within the previous experiment and were stored in a deep freezer at −80°C. The samples were then dissolved in 1 mL of sterile PBS (phosphate-buffered solution), filtered three times with a 100μm sterile filter in order to remove impurities, and centrifuged at 4°C at 3,000 rpm for 10 minutes to prepare a fecal bacteria solution with a concentration of 100 mg/mL. The supernatant was then drawn into a 5 mL sterile EP (Eppendorf) tube. The recipient mice were given an intragastric gavage every four days, each at 200 μL, for a total of eight weeks.

Alveolar Lavage Fluid

After the mice were euthanized with an overdose of anesthetic. A 20G indwelling needle was inserted into the trachea in order to fix the trachea, and a 1 mL syringe was used to draw 0.3 mL of normal saline into the lungs. After repeated washing (three times), the fluid was recovered into the centrifuge tube and the normal salt solution was drawn again for perfusion. The above procedure was repeated three times. After centrifugation, the supernatant was aspirated and the sample was stored in a −80°C deep freezer. The cell sediment was resuspended in 100 μL PBS; 25 μL was then transferred to the automatic blood cell analyzer (model: XS-800i, Sysmex) in order to obtain the total cell counts as well as to characterize the various types of cells present in the sample.

Histological Evaluation

After the mice were euthanized, their lungs were removed, fixed with 10% formaldehyde solution, sliced, and stained with hematoxylin and eosin (HE). Histological examination was then performed. The mean linear intercept (MLI) of the lungs was tested and evaluated for emphysema using Image Pro Plus software (Media Cybernetics, Inc., Rockville, MD, USA). At least three random fields of view were examined for each mouse.

Cytokines and Neutrophil Enzymes Level

The levels of the serum cytokines (IL-6, IL-8, TNF-a, HMGB1) and neutrophil enzymes (MPO, NE) were detected according to ELISA (enzyme-linked immunoassay) kit instructions (MALLBIO, Nanjing, China).

Quantitative Real-Time PCR

Referring to the reagent instructions, total RNA was extracted from lung tissue using TRIzol reagent (Ambion, Austin, TX, USA). A reverse transcription kit (Vazyme, Nanjing, China) was used to synthesize cDNA from total RNA. The sequence-specific primers for HMGB1 and RAGE are shown in Table 1. A 7500 Fast PCR machine was used for

Table 1 Primer Sequence Information

Gene name	Forward primer (5′–3′)	Reverse primer (5′–3′)
HMGB1	AGATATGGCAAAGGCTGACAAGGC	GGGCGGTACTCAGAACAGAACAAG
RAGE	CTACCTTCTCCTGCAGTTTCAG	CATCCTTTATCCAGTGGACCTG
GAPDH	AGCAGTCCCGTACACTGGCAAAC	TCTGTGGTGATGTAAATGTCCTCT

conducting the amplification reaction (Thermo Fisher Scientific, Waltham, MA, USA). A standard formula ($2^{-\Delta\Delta Ct}$) was used to calculate the expression level of the target gene relative to that of the endogenous control gene.

Intestinal Flora DNA Extraction and PCR Amplification

According to the E.Z.N.A.® soil DNA kit manual (Omega Bio-Tek, Norcross, GA, USA), the total DNA of the microbial community was extracted, and the concentration and purity were determined using NanoDrop 2000 (Thermo Fisher Scientific). Bacterial genomic DNA was PCR amplified with 338F (5′-ACTCCTACGGGAGGCAGCAG-3′) and 806R (5′-GGACTACHVGGGTWTCTAAT-3′) primers within the 16S rRNA gene V3-V4 variable region.

Illumina Miseq Sequencing

A Quantus™ Fluorometer (Promega, Madison, WI, USA) was used to detect and quantify PCR products. A NEXTFLEX Rapid DNA-Seq Kit (PerkinElmer Applied Genomics, Waltham, MA, USA) was used to build the library. Sequencing was performed using the Illumina Miseq PE300 platform (Shanghai Meiji Biomedical Technology Co., Ltd., Shanghai, China).

SCFA (Short Chain Fatty Acids) Quantitative Evaluation

Stool sample preparation was conducted using 100 mg feces sample and 1 mL of water (mixed 0.5% phosphoric acid and 50 μg/mL 2-methyl butyric acid), and the sample was ground twice in a cryo-milling machine. We then performed ultrasound in an ice-water bath for 30 min and left the sample out for 30 minutes at a room temperature of 4°C. We then placed the sample in a centrifuge at 4°C, performed centrifuging at 13,000 g for 15 minutes, collected the supernatant, added 500 μL of ethyl acetate to the supernatant, and vortexed the sample to mix the contents, followed by sonication in an ice-water bath for 10 minutes, centrifugation at 13,000 g for 10 minutes at 4°C, and aspiration of the supernatant for subsequent analysis.

According to the implemented formula (short-chain fatty acid content (μg/mg) = (C*V)/M), the contents of the metabolites in the sample were calculated based on the standard curve and the detection concentration of the sample (C: computer concentration, V: constant volume, M: sample weight). The ion fragments of the short-chain fatty acids in the sample were identified and integrated using Masshunter quantitative software (Agilent) and were also manually detected.

Statistical Analysis

GraphPad Prism 8 software (San Diego, CA, USA) was used to organize and analyze the experimental data. The measurement data were expressed as Means ± standard deviations. Intergroup comparisons were performed using single-factor or two-factor analysis of variance, and $P<0.05$ was considered the threshold for statistical significance. Each independent experiment was repeated three times.

Results

Effects of Emodin on Body Weight and Inflammatory Cells

Experiment 1 evaluated the effects of emodin on COPD based on the establishment of a COPD mouse model. Compared with the control group, the weight of the mice in the COPD group gradually decreased, while the weight of the mice treated with emodin increased compared with the model group (Figure 1a). After modeling, the number of neutrophils in the alveolar lavage fluid of the evaluated mice increased statistically significantly, and the NLR likewise increased. After emodin treatment, neutrophil counts in the alveolar lavage fluid and the NLR showed a downward trend (Figure 1b).

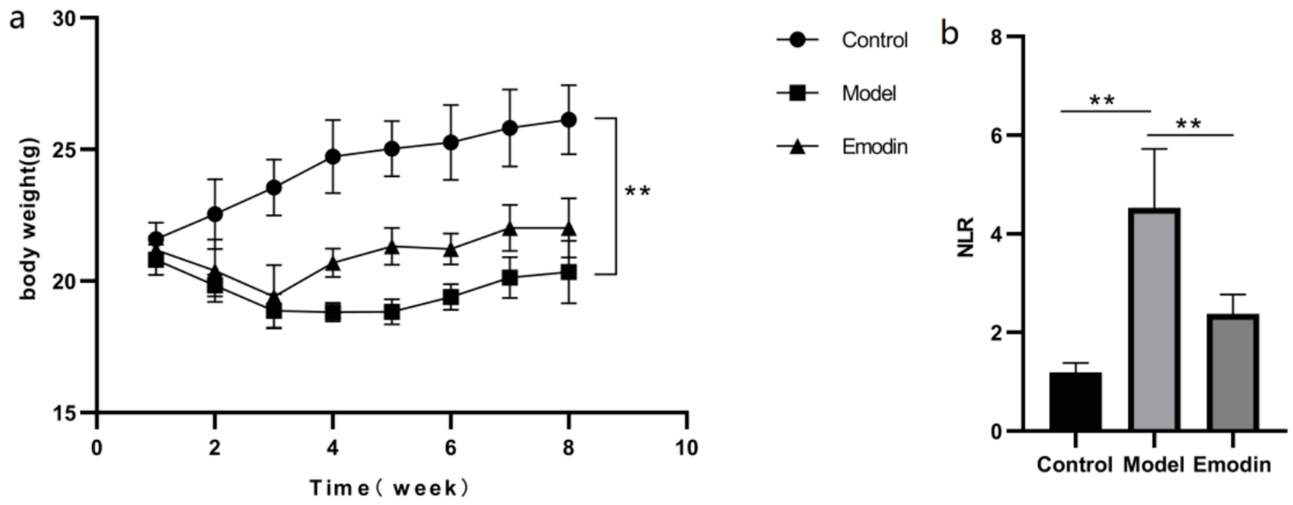

Figure 1 Effects of emodin on body weight and inflammatory cell counts. (**a**) Body weight of mice in each group. Values are expressed as means ± standard deviations (SD). (**b**) NLR (neutrophil to lymphocyte ratio) values in the alveolar lavage fluid of each group of mice. $^{**}P < 0.01$.

Emodin-Attenuated Pathological Changes in the Lung Tissue of COPD Mice

Compared with the control group, smoking and intratracheal instillation of LPS caused inflammatory cell infiltration in lung tissue, destruction of the alveolar structure (Figure 2a and b), and an increase in the MLI (Figure 2d), After emodin treatment, the inflammation and emphysema of the lung tissue were statistically significantly reduced (Figure 2c and d).

Effects of Emodin on Inflammatory Cytokines and Neutrophil Enzymes

The levels of inflammatory cytokines (IL-6, IL-8, TNF-a and HMGB1) and neutrophil enzymes (MPO, NE) in the serum of COPD mice were statistically significantly higher than those in the control group, suggesting that this finding was related to the presence of inflammatory cells, especially with regard to neutrophil infiltration. The levels of IL-6, IL-8, TNF-a, MPO, NE, and HMGB1 in the emodin group were found to decrease ($P<0.05$) (Figure 3a–f).

Effects of Emodin on HMGB1 and RAGE mRNA Expression Levels

Compared with the control group, the relative expression levels of HMGB1 and RAGE mRNA in the lung tissue of the model group were statistically significantly increased. After emodin treatment, the expression levels of HMGB1 and RAGE mRNA were down-regulated, as shown in Figure 4a and b. The results of Experiment 1 show that emodin reduced the degree of COPD inflammation and had a regulatory effect on the HMGB1-RAGE inflammation pathway.

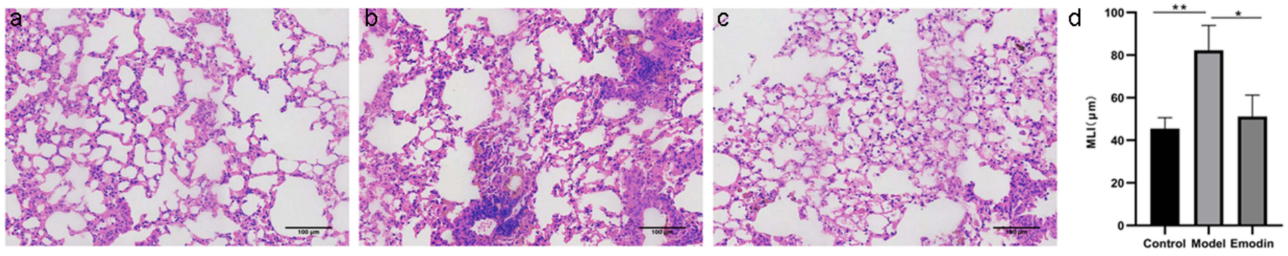

Figure 2 Emodin attenuated the pathological changes in the lung tissue of the COPD (chronic obstructive pulmonary disease) mice. (**a–c**). Hematoxylin and eosin (HE) pathological map of mice in each group (×100). (**a**) Control group. (**b**) COPD group. (**c**) Emodin group. (**d**) The mean lining interval (MLI) of each group of mice. $^{*}P < 0.05$ and $^{**}P < 0.01$.

https://doi.org/10.2147/JIR.S532395

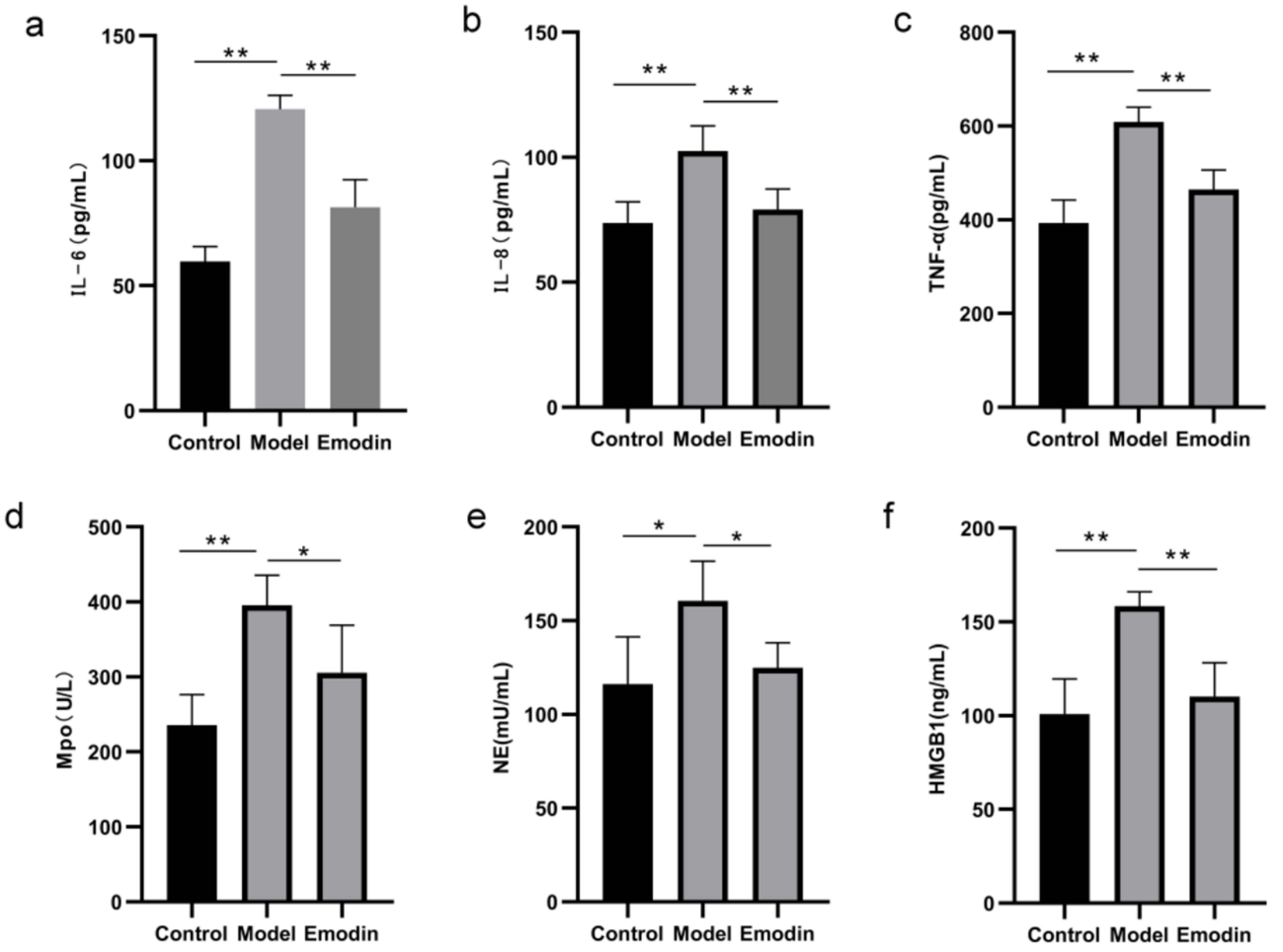

Figure 3 Serum levels of inflammatory cytokines (TNF-a, IL-6, IL-8, HMGB1) and neutrophil enzymes (MPO, NE). (**a**) Serum levels of IL-6. (**b**) Serum levels of IL-8. (**c**) Serum levels of TNF-a. (**d**) Serum levels of MPO. (**e**). Serum levels of NE. (**f**) Serum levels of HMGB1. *P <0.05 and **P <0.01.

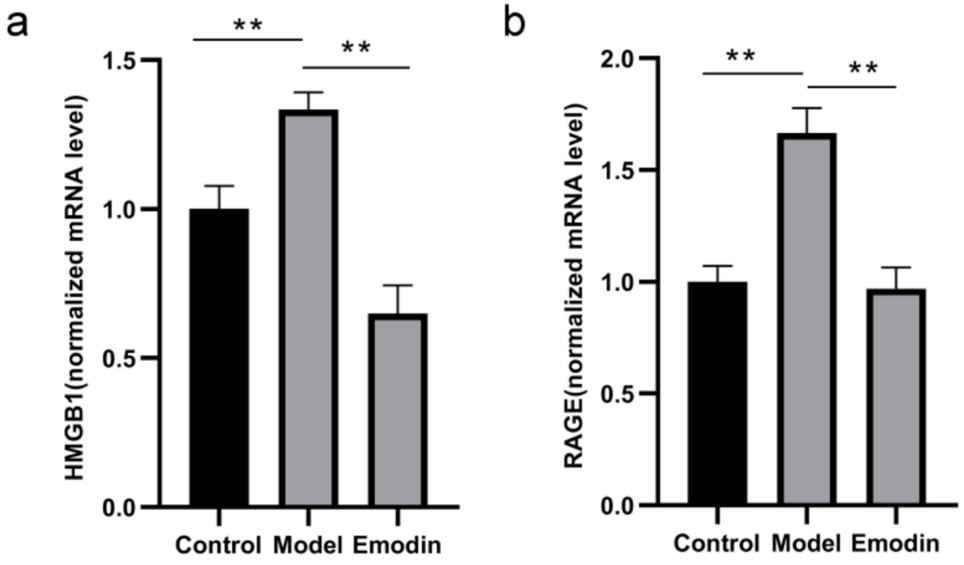

Figure 4 Effects of emodin on the expression level of HMGB1 (high mobility group box protein 1) mRNA and RAGE (receptor for advanced glycation end-products) mRNA. (**a**) Expression level of HMGB1 mRNA. (**b**) Expression level of RAGE mRNA. **P < 0.01.

Effects of Emodin on Intestinal Flora

The point of action of emodin in Chinese medicine is with regard to the interface of the lung and large intestine. Based on the results of Experiment 1, we speculate that emodin can affect the composition of intestinal microbes as well as associated metabolites.

The PCA analysis showed that, as depicted in Figure 5a, the COPD model group had a unique microbial community structure as compared with the control group of mice, and that this structure was clearly distinguished from the emodin group and the control group. The differences in each group of microorganisms were further analyzed at the phylum and family level, as shown in Figure 5b and c. At the phylum level, *Firmicutes* and *Bacteroides* were the main microbiota found in the feces. *Firmicutes* was the most dominant bacterial species in the stool samples of COPD mice. *Bacteroides* accounted for the largest proportion of bacterial species in mice in the emodin group. The remaining differential flora are as depicted in Figure 5b. At the family level, as compared with the control group of mice, COPD mice showed statistically significantly increased levels of *Muribaculaceae* and *Erysipelotrichaceae* as well as decreased levels of *Lachnospiraceae* and *Bifidobacteriaceae*. Compared with mice in the COPD group, mice in the emodin group had increased *Muribculaceae, Bifidobacteriaceae, Desulfovibrionaceae*, and *Akkermansiaceae* levels and decreased *Erysipelotrichaceae, Lachnospiraceae*, and *Lactobacillaceae* levels. The remaining differential flora are as depicted in Figure 5c.

Effects of Emodin on SCFA

The eight short-chain fatty acids with the highest content are as shown in Figure 6. The top three fatty acids with regard to statistical significance were acetic acid, propanoic acid, and butanoic acid (Figure 6a–c). The contents of acetic acid, propionic acid, and butyric acid in the model group were statistically significantly reduced. Compared with the model group, the acetic acid content of the emodin group showed a downward trend, while propionic acid and butyric acid both increased at the level of statistical significance. The remaining SCFA content was as shown in Table 2.

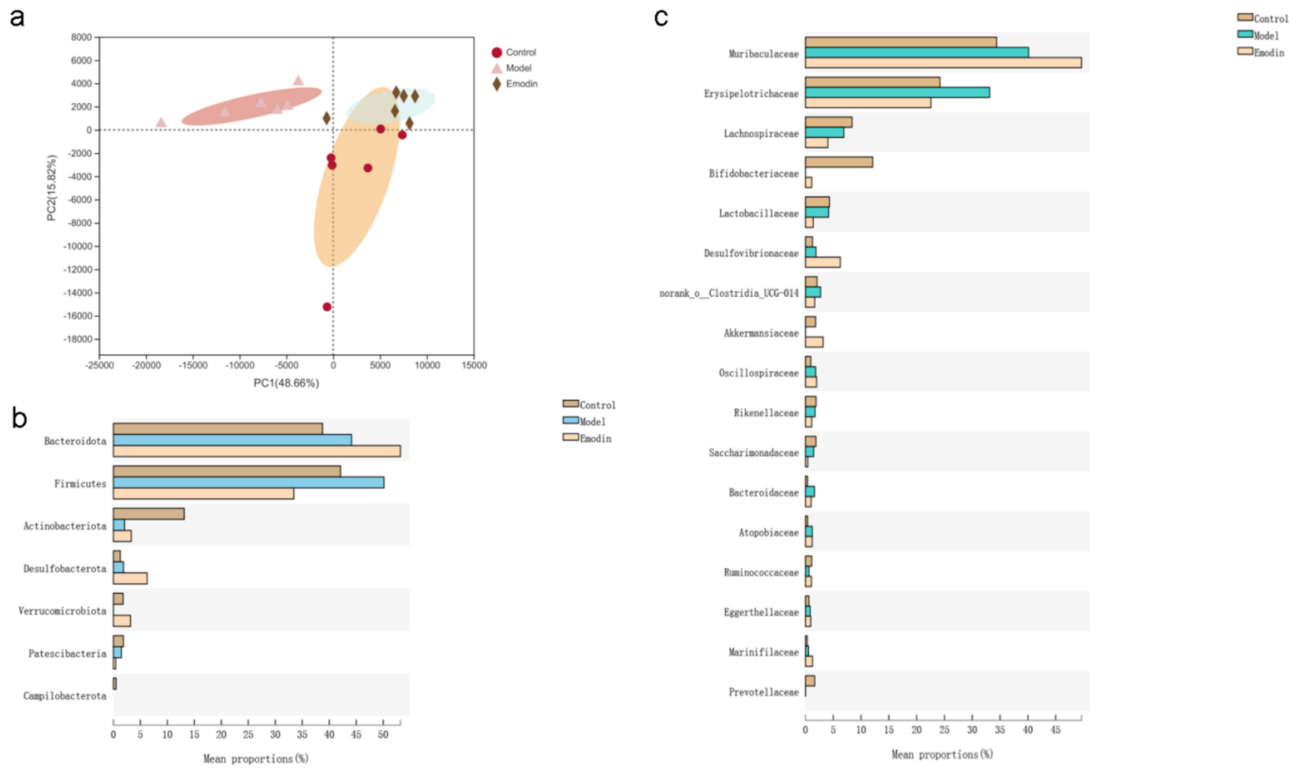

Figure 5 Effects of emodin on the intestinal flora. (**a**) The results of a principal component analysis (PCA). (**b**). Tests of differences between multiple groups (at the phylum level). (**c**) Tests of differences between multiple groups (at the family-level).

https://doi.org/10.2147/JIR.S532395

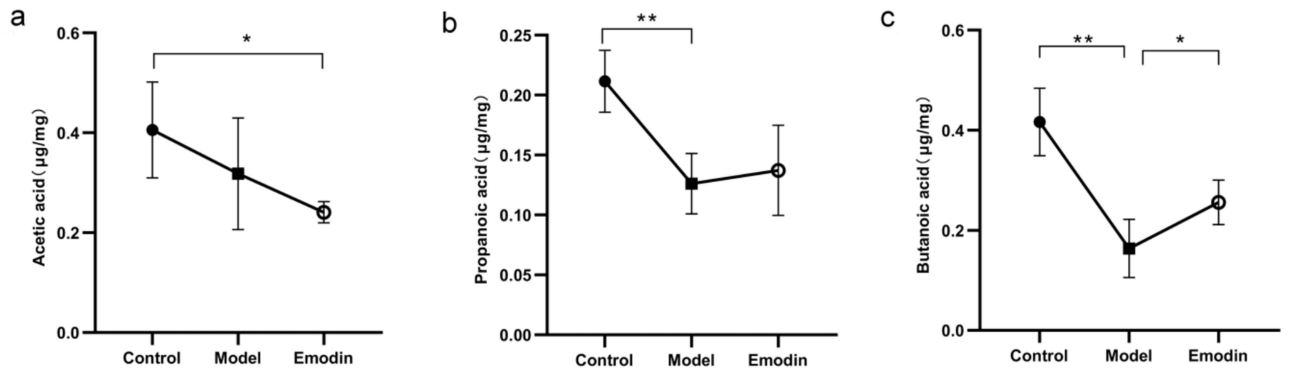

Figure 6 Acetic acid, propionic acid, and butyric acid content in each group. (**a**) Acetic acid. (**b**) Propionic acid. (**c**) Butyric acid. $^{**}p<0.01$, $^{*}p<0.05$.

Correlation Analysis of Intestinal Flora and SCFA

To further analyze the relationship between the bacterial flora and metabolites in each group, an RDA (redundancy) analysis was used to observe the correlation between short-chain fatty acids and flora at the level of OUT (Operational Taxonomic Units) (Figure 7). It can be seen from the figure that the butanoic acid level clearly distinguished the model group from the other groups, indicating that butanoic acid had a more meaningful impact on the distribution of flora.

Verification of the Flora Depletion Model

The feces of mice receiving antibiotic drinking water were analyzed by 16S rRNA sequencing, and a pie chart of the community composition in the feces was obtained (compared with the control group of mice, Figure 8a and b). At the family level, the group of mice in the control group consisted of *Muribaculaceae, Erysipelotrichaceae*, and *Bifidobacteriaceae. Enterobacteriaceae* were not detected. After antibiotic gavage, *Enterobacteriaceae* accounted for 77.99% of the mouse fecal community composition. The diversity of the flora was statistically significantly reduced, antibiotic-related pathogenic bacteria were found to dominate, and the flora depletion model was thus concluded to be successfully established.

Effects of FMT on Body Weight and Inflammatory Cells

Based on the bacterial depletion model, Experiment 2 was carried out in order to observe the influence of FMT on COPD. The body weight of the mice in the double model group (bacterial depletion + COPD modeling) decreased statistically significantly after depletion of the intestinal flora and then slowly increased, while the weight of the mice receiving the emodin flora transplantation treatment increased compared with that of the model group (Figure 9a). The number of neutrophils in the alveolar lavage fluid of the two-module mice increased statistically significantly, and the lymphocytes were increased as well. The number of neutrophils in the alveolar lavage fluid of the emodin transplantation group showed a downward trend. The lymphocytes were all decreased as compared with the control group, and the NLR likewise decreased (Figure 9b).

Effects of FMT on Lung Tissue in COPD Mice

Bacterial depletion + COPD modeling resulted in the infiltration of inflammatory cells in lung tissue, destruction of the alveolar structure (Figure 10a and b), and an increase in the MLI (Figure 10d). After transplanting the feces of the emodin group, lung tissue inflammation and emphysema were found to be statistically significantly reduced (Figure 10c and d).

Table 2 Short-Chain Fatty Acid Content Values

Group	Acetic Acid	Propionic Acid	Butyric Acid	Isobutyric Acid	Valeric Acid	Isovaleric Acid	Hexanoic Acid	Isohexanoic Acid
Control	0.40580±0.09615	0.21160±0.02583	0.41670±0.06731	0.02103±0.00832	0.06378±0.02313	0.01433±0.00501	0.00343±0.00448	0.00028±0.00069
D model	0.31820±0.11180	0.12610±0.02518	0.16360±0.05824	0.01538±0.00684	0.04562±0.01757	0.01177±0.00520	0.00137±0.00129	0.00025±0.00036
Emodin	0.24090±0.02116	0.13730±0.03766	0.25570±0.04437	0.01572±0.00509	0.04868±0.01008	0.01313±0.00380	0.00100±0.00046	0.00018±0.00045

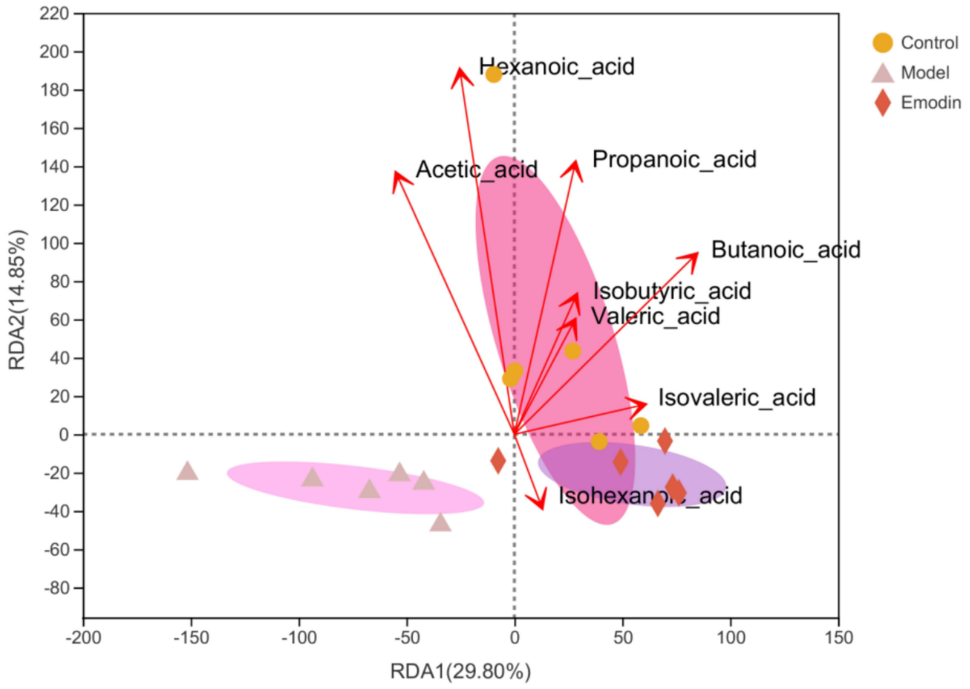

Figure 7 Correlation analysis between intestinal flora and short-chain fatty acids. Triangles, diamonds, and circles represent different samples. The red arrows represent 8 types of short chain fatty acids. The length of the arrow represents the degree of impact of short chain fatty acids on species, the angle of the arrow represents correlation, acute angle represents positive correlation, obtuse angle represents negative correlation, and right angle represents non correlation. Project the sample onto the arrow line, and the distance from the projection point to the origin represents the relative impact of short chain fatty acids on the distribution of the sample community.

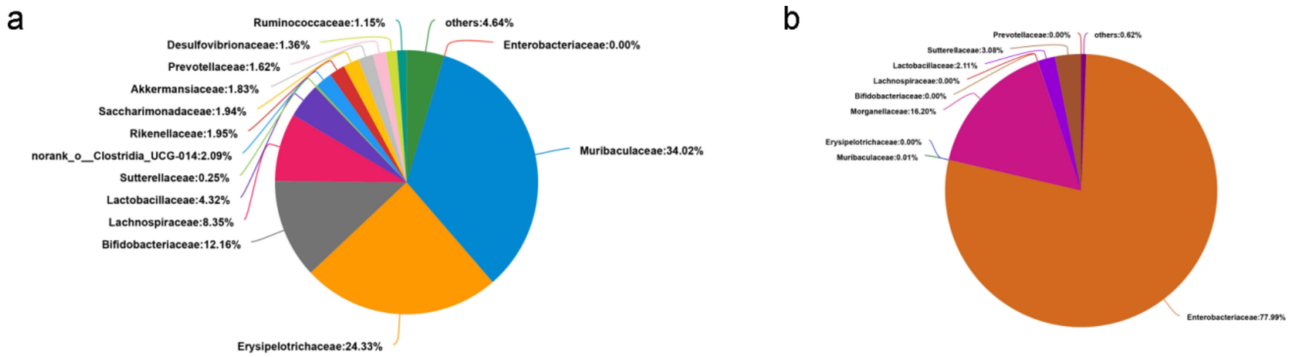

Figure 8 Fecal microbial community composition of normal mice and antibiotic mice. (**a**) Normal mice. (**b**) Antibiotic mice.

Effect of FMT on Inflammatory Cytokines and Neutrophil Enzymes

The levels of inflammatory cytokines (IL-6, IL-8, TNF-a and HMGB1) and neutrophil enzymes (MPO, NE) in the serum of the double module (bacterial depletion + COPD modeling) mice were statistically significantly higher than those in the control group, and the levels of the above-mentioned cytokines and neutrophil enzymes in the emodin transplantation group were statistically significantly reduced (Figure 11a–f).

Effects of FMT on HMGB1mRNA and RAGE mRNA Expression

Compared with the control group, the expression levels of HMGB1 and RAGE mRNA in the lung tissue of the double model (bacterial depletion + COPD modeling) mice were statistically significantly increased. Compared with the double model group, the expression levels of HMGB1 and RAGE mRNA in the emodin transplantation group were down-regulated (Figure 12a and b).

https://doi.org/10.2147/JIR.S532395

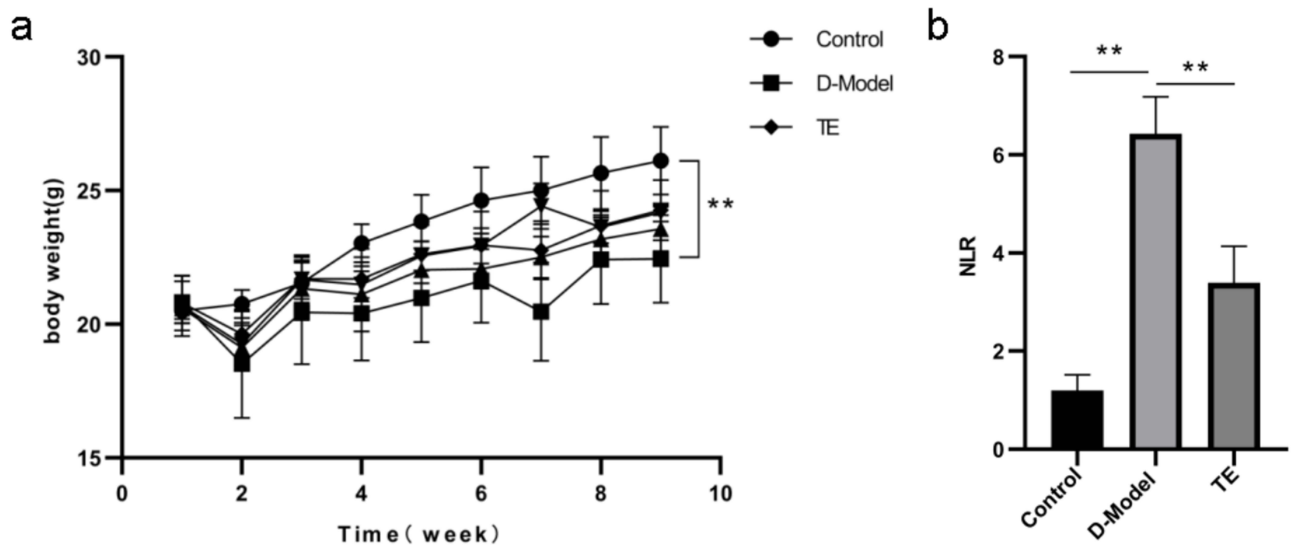

Figure 9 Effects of fecal microbiota transplantation (FMT) on body weight and inflammatory cell counts. (**a**) Body weight of the mice in each group. Values are expressed as means ± standard deviations (SD). $^{**}P < 0.01$. (**b**). Neutrophil to lymphocyte ratio (NLR) values in the alveolar lavage fluid of each group of mice. $^{**}P < 0.01$.

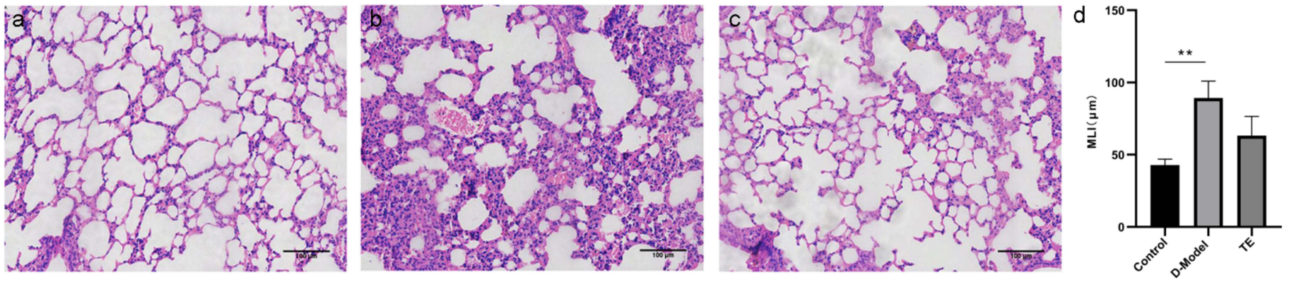

Figure 10 Effect of fecal microbiota transplantation (FMT) on the lung tissue of COPD mice. a-c. Hematoxylin and eosin (HE) pathological map for the mice in each group (×100). (**a**). Control group. (**b**). Double model (D-model) group. (**c**). Transplanted emodin (TE) group. (**d**) Comparison of the mean lining interval (MLI) for each group of mice. $^{**}P < 0.01$.

Discussion

Smoking is the primary cause of COPD. Chronic persistent inflammation is the primary characteristic of the COPD disease process.[8] Existing animal experimental models have shown that cigarettes cause a continuous inflammatory response.[9,10] Lipopolysaccharide (LPS) is a pro-inflammatory component in the cell wall of Gram-negative bacteria. It combined with cigarette smoke is an established method used to simulate the process of COPD.[11,12]

In this experiment, cigarettes combined with LPS tracheal installation were used to establish a COPD mouse model. The pathological results showed that the lung tissue of these models presented with obvious inflammation, indicating that the model was successfully established.

Neutrophils are the most important inflammatory cells in the pathological mechanisms of COPD.[13] The lifespan of neutrophils is very short. However, in the process of COPD development and aggravation, viral and/or bacterial infections, oxidative stress, and upregulation of IL-8, NF-κB, and IL-6 limit the clearance of macrophages, inhibit the spontaneous apoptosis of neutrophils.[14] The surviving neutrophils still have normal chemotaxis and pro-inflammatory functions, thereby leading to permanent airway inflammation and tissue damage.[15]

Lymphocytes reflect the immune function of the body, and the ratio of neutrophils to lymphocytes can reflect the level of inflammation in the body.[16] The higher the NLR level, the stronger the inflammatory response in the body and the more severe the patient's condition.[17,18] The results of our experiment demonstrated that the neutrophil count in the alveolar lavage fluid of mice in the COPD model group was statistically significantly higher than that in the control group. The NLR was statistically

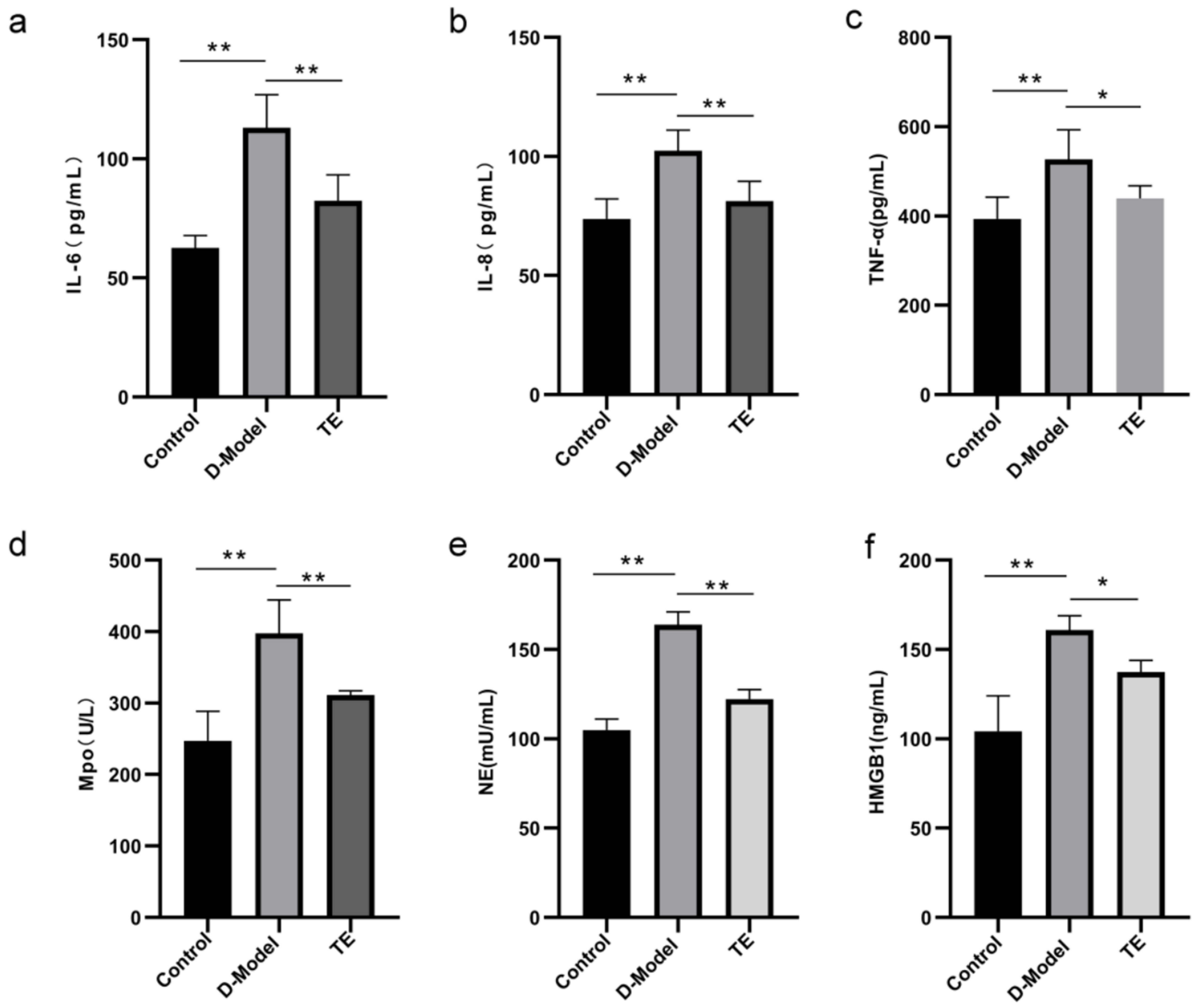

Figure 11 Effects of fecal microbiota transplantation (FMT) on the levels of inflammatory cytokines (TNF-a, IL-6, IL-8, HMGB1) and neutrophil enzymes (MPO, NE). (**a**). Serum levels of IL-6. (**b**) Serum levels of IL-8. (**c**) Serum levels of TNF-a. (**d**) Serum levels of MPO. (**e**). Serum levels of NE. (**f**). Serum levels of HMGB1. *$P < 0.05$ and **$P < 0.01$.

significantly higher than that in the control group (P<0.05), which was in line with the pathophysiological changes seen in COPD development, aggravation, and progression. After treatment with emodin, the NLR as statistically significantly decreased.

RAGE was evaluated as a model receptor. It bound to ligands such as AGEs, HMGB1 and S100 and plays an important role in a variety of disease processes.[19] Studies have shown that RAGE is involved in the pathogenesis of COPD, mediating the destruction of lung parenchyma caused by cigarette smoke and eventually causing emphysema.[20] HMGB1 is the ligand with the highest affinity for RAGE, it not only participates in DNA transcription, but also acts as an extracellular signal mediator to regulate inflammatory factors, chemokines, and reactive oxygen species, thus leading to inflammatory reactions and tissue damage.[21] In addition, HMGB1 has been confirmed to be an inhibitor of the Bcl-2 family Bak protein, which can antagonize cell apoptosis induced by Casp8 and Bax.[22] A clinical study on the level of HMGB1 in the sputum and blood of patients with COPD and asthma found that HMGB1 had a higher expression level in the sputum of patients with COPD, and was likewise negatively correlated with lung function and neutrophil counts.[23] HMGB1 plays a role in recruiting neutrophils, and the HMGB1-RAGE axis selectively regulates the migration of neutrophils to necrotic tissue.[24] The PI3K/Akt pathway, which is downstream of HMGB1-RAGE, plays an important role in the transmission of neutrophil anti-apoptotic signals, which can in turn directly promote inflammation and cause delayed apoptosis of lung neutrophils.[25]

https://doi.org/10.2147/JIR.S532395

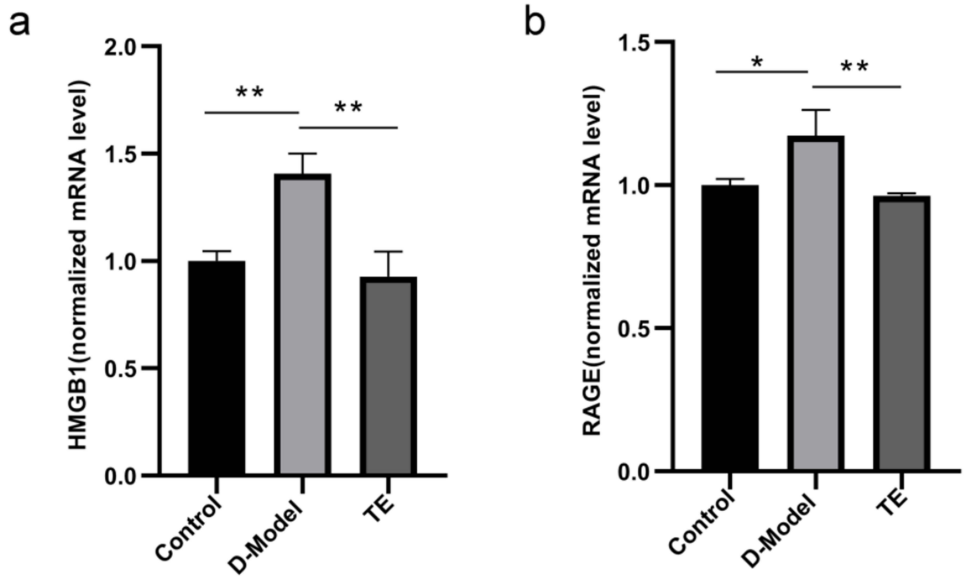

Figure 12 Effects of fecal microbiota transplantation (FMT) on the expression of HMGB1 (high mobility group box protein 1) and RAGE (receptor for advanced glycation end-products) mRNA. (**a**) Expression level of HMGB1 mRNA. (**b**) Expression level of RAGE mRNA. $^{**}P < 0.05$ and $^{*}P < 0.01$.

In modern medicine, the lung and the large intestine are known to be linked by the intestinal flora and metabolites.[26] Therefore, this experiment mainly focused on studying the effects of emodin on the short-chain fatty acid metabolites of the intestinal flora for the purpose of evaluating the mechanism of treating the lung from the intestine and laying the experimental foundation for clinical application.

The traditional way of administering Chinese medicine is through oral decoctions, which are absorbed by the digestive tract before taking effect. Advances in genomic sequencing technology have gradually revealed the role of intestinal flora, and changes in microbial metabolites have become a new observation point for assessing the efficacy of traditional Chinese medicine.[27] Intestinal microorganisms can transform Chinese medicine components into metabolites with different biological activities, and at the same time regulate the interaction of chemical substances in Chinese medicine. For example, a study on the treatment of type 2 diabetes mellitus (T2D) with Gegen Qinlian Decoction (GQD) showed that different doses of GQD showed dose-dependent deviation in the sequencing of 16S rRNA gene of intestinal microorganisms, which was corresponding to the improvement of symptoms, and the change of intestinal microflora was related to the anti-diabetic effect of GQD. Research on the gut-pulmonary axis has found that during COPD pathogenesis, patients exhibit alterations in the metabolic environment of intestinal microbes, which in turn induces the occurrence or exacerbation of COPD.[28]

SCFAs mainly including acetic acid, propionic acid, butyric acid, valeric acid, and caproic acid.[29] SCFAs receptors such as GPR109A, GPR41, and GPR43 are widely distributed in endocrine cells, immune cells, and intestinal epithelial cells and are involved in the regulation of metabolism, immunity, and inflammation.[30,31]

Acetic acid and propionic acid are mostly absorbed through the intestinal tract and act as regulators of energy metabolism.[32] They affect the glucose metabolism process in the liver and provide energy for the liver.[33]

As a histone deacetylase inhibitor, butyric acid regulates epigenetic gene expression,[34] and plays an anti-inflammatory role through effects on NF-κB.[35] At the same time, butyric acid is an effective inhibitor of HMGB1. In acute lung inflammatory disease models, butyric acid has been found to inhibit MPO activity in mice, reduce TNF-α and IL-6 levels, and reduce inflammatory cell aggregation.[36]

The results of this experiment demonstrated that emodin affected the HMGB1-RAGE pathway and down-regulated the mRNA expression of the pro-inflammatory factor HMGB1 and its receptor (RAGE). After treatment with emodin, the neutrophil counts and the NLR in the alveolar lavage fluid of the evaluated mice were statistically significantly reduced, and the lung tissue pathology was likewise statistically significantly reduced as compared with the model group. Thus, it can be seen that emodin regulated the apoptosis process through the HMGB1-RAGE pathway and reduced the inflammatory response in the COPD model mice. The results of the short-chain fatty acid evaluation indicated that the contents of acetic

acid, propionic acid, and butyric acid in the model group were statistically significantly reduced, with butyric acid showing the most statistically significant change. After emodin treatment, acetic acid decreased, the propionic acid content was higher than that of the model group, and the butyric acid content was statistically significantly increased.

Fecal microbiota transplantation is a treatment methodology developed with the goal of affecting the composition of intestinal microbiota.[37] With regard to the treatment of COPD, FMT has also been preliminarily confirmed as a possible method for delaying the progression of emphysema through inhibiting inflammation and changing the structure of the intestinal flora.[38]

To further clarify the role of intestinal flora in the treatment of COPD with emodin, we used antibiotics in order to establish a microbiota depletion mouse model, thus pre-excluding the influence of the microbiota. After transplantation, the general condition of the evaluated mice as well as lung tissue pathology and the alveolar lavage fluid inflammatory cell count analysis showed that the transplanted mice treated with emodin showed statistically significantly improved lung inflammation as well as reduced the infiltration of inflammatory cells in the lesion. Compared with COPD model mice, we detected more severe lung inflammation in double model (bacterial depletion + COPD modeling).

Our results indicated that the expression of HMGB1 and RAGE mRNA in the lung tissue of mice in the bacterial depletion model group were statistically significantly increased, while the above indicators showed the opposite trend for the emodin bacterial transplantation group.

This experiment has provided critically important ideas for follow-up research, but there are many shortcomings of our research. For example, the evidence chain was not perfect and needs further supplementation. Our findings, however, provide critical information for guiding future research.

Conclusion

Emodin exerts dual therapeutic effects on COPD: it not only mitigates pulmonary neutrophil infiltration and alleviates pathological damage by modulating associated signaling pathways, but also restructures gut microbiota composition. Resulting microbial metabolites subsequently promote resolution of pulmonary inflammation. These findings provide critical insights for elucidating mechanisms of the gut-pulmonary axis and guiding future research directions.

Data Sharing Statement

Raw data used for analysis are available in a Zenodo repository: https://sandbox.zenodo.org/records/185593.

Ethics Statement

Procedures operated in this research were completed in keeping with the standards set out in the Announcement of Helsinki and laboratory guidelines of research in China.

Author Contributions

All authors made a significant contribution to the work reported, whether that is in the conception, study design, execution, acquisition of data, analysis and interpretation, or in all these areas; took part in drafting, revising or critically reviewing the article; gave final approval of the version to be published; have agreed on the Journal of Inflammation Research to which the article has been submitted; and agree to be accountable for all aspects of the work.

Funding

This study was supported by the Special Research Project of the National Clinical Research Base of Traditional Chinese Medicine (No. 2022JDZX126) and Natural Science Foundation of Henan (No. 242300420430; 252300420620).

Disclosure

The authors declare that the research was conducted in the absence of any commercial or financial relationships that could be construed as a potential conflict of interest.

References

1. Sidhaye VK, Nishida K, Martinez FJ. Precision medicine in COPD: where are we and where do we need to go? *Eur Respir Rev*. 2018;27 (149):180022. doi:10.1183/16000617.0022-2018
2. V Feigin. Global, regional, and national incidence, prevalence, and years lived with disability for 310 diseases and injuries, 1990-2015: a systematic analysis for the Global Burden of Disease Study 2015. *Lancet*. 2016;388(10053):1545–1602. doi:10.1016/s0140-6736(16)31678-6
3. Xue J, Shi S. Exploration of the Potential Mechanisms of Compounds from Rheum palmatum L. against Chronic Obstructive Pulmonary Disease: a Network Pharmacology Study. *Comb. Chem. High Throughput Screening*. 2021;24(7):1093–1113. doi:10.2174/1386207323666200901095541
4. Poto R, Loffredo S, Palestra F, Marone G, Patella V, Varricchi G. Angiogenesis, Lymphangiogenesis, and Inflammation in Chronic Obstructive Pulmonary Disease (COPD): few Certainties and Many Outstanding Questions. *Cells*. 2022;11(10):1720. doi:10.3390/cells11101720
5. Feng F, Du J, Meng Y, Guo F, Feng C. Louqin Zhisou Decoction Inhibits Mucus Hypersecretion for Acute Exacerbation of Chronic Obstructive Pulmonary Disease Rats by Suppressing EGFR-PI3K-AKT Signaling Pathway and Restoring Th17/Treg Balance. *Evid Complement Alternat Med*. 2019;2019:6471815. doi:10.1155/2019/6471815
6. Cervilha DAB, Ito JT, Lourenço JD, et al. The Th17/Treg Cytokine Imbalance in Chronic Obstructive Pulmonary Disease Exacerbation in an Animal Model of Cigarette Smoke Exposure and Lipopolysaccharide Challenge Association. *Sci Rep*. 2019;9(1):1921. doi:10.1038/s41598-019-38600-z
7. Starkey MR, Jarnicki AG, Essilfie AT, et al. Murine models of infectious exacerbations of airway inflammation. *Curr Opin Pharmacol*. 2013;13 (3):337–344. doi:10.1016/j.coph.2013.03.005
8. de Oliveira MV, Rocha NN, Santos RS, et al. Endotoxin-Induced Emphysema Exacerbation: a Novel Model of Chronic Obstructive Pulmonary Disease Exacerbations Causing Cardiopulmonary Impairment and Diaphragm Dysfunction. *Front Physiol*. 2019;10:664. doi:10.3389/fphys.2019.00664
9. Meijer M, Rijkers GT, van Overveld FJ. Neutrophils and emerging targets for treatment in chronic obstructive pulmonary disease. *Expert Rev Clin Immunol*. 2013;9(11):1055–1068. doi:10.1586/1744666x.2013.851347
10. Brown V, Elborn JS, Bradley J, Ennis M. Dysregulated apoptosis and NFkappaB expression in COPD subjects. *Respir Res*. 2009;10(1):24. doi:10.1186/1465-9921-10-24
11. Porto BN, Stein RT. Neutrophil Extracellular Traps in Pulmonary Diseases: too Much of a Good Thing? *Front Immunol*. 2016;7:311. doi:10.3389/fimmu.2016.00311
12. Farah R, Ibrahim R, Nassar M, Najib D, Zivony Y, Eshel E. The neutrophil/lymphocyte ratio is a better addition to C-reactive protein than CD64 index as a marker for infection in COPD. *Panminerva Med*. 2017;59(3):203–209. doi:10.23736/s0031-0808.17.03296-7
13. Liu J, Liu J, Zou Y. Relationship between neutrophil-lymphocyte ratio and short-term prognosis in the chronic obstructive pulmonary patients with acute exacerbation. *Biosci Rep*. 2019;39(5):675. doi:10.1042/bsr20190675
14. Yao C, Liu X, Tang Z. Prognostic role of neutrophil-lymphocyte ratio and platelet-lymphocyte ratio for hospital mortality in patients with AECOPD. *Int J Chron Obstruct Pulmon Dis*. 2017;12:2285–2290. doi:10.2147/copd.S141760
15. Hudson BI, Lippman ME. Targeting RAGE Signaling in Inflammatory Disease. *Annu Rev Med*. 2018;69(1):349–364. doi:10.1146/annurev-med-041316-085215
16. Sanders KA, Delker DA, Huecksteadt T, et al. RAGE is a Critical Mediator of Pulmonary Oxidative Stress, Alveolar Macrophage Activation and Emphysema in Response to Cigarette Smoke. *Sci Rep*. 2019;9(1):231. doi:10.1038/s41598-018-36163-z
17. Feng X, Wu C, Yang M, et al. Role of PI3K/Akt signal pathway on proliferation of mesangial cell induced by HMGB1. *Tissue Cell*. 2016;48 (2):121–125. doi:10.1016/j.tice.2015.12.007
18. Brezniceanu ML, Völp K, Bösser S, et al. HMGB1 inhibits cell death in yeast and mammalian cells and is abundantly expressed in human breast carcinoma. *FASEB j*. 2003;17(10):1295–1297. doi:10.1096/fj.02-0621fje
19. Hou C, Zhao H, Liu L, et al. High mobility group protein B1 (HMGB1) in Asthma: comparison of patients with chronic obstructive pulmonary disease and healthy controls. *Mol Med*. 2011;17(7–8):807–815. doi:10.2119/molmed.2010.00173
20. Huebener P, Pradere JP, Hernandez C, et al. The HMGB1/RAGE axis triggers neutrophil-mediated injury amplification following necrosis. *J Clin Invest*. 2015;125(2):539–550. doi:10.1172/jci76887
21. Zhao H, Ma Y, Zhang L. Low-molecular-mass hyaluronan induces pulmonary inflammation by up-regulation of Mcl-1 to inhibit neutrophil apoptosis via PI3K/Akt1 pathway. *Immunology*. 2018;155(3):387–395. doi:10.1111/imm.12981
22. Yue SJ, Wang WX, Yu JG, et al. Gut microbiota modulation with traditional Chinese medicine: a system biology-driven approach. *Pharmacol Res*. 2019;148:104453. doi:10.1016/j.phrs.2019.104453
23. Tan J, McKenzie C, Potamitis M, Thorburn AN, Mackay CR, Macia L. The role of short-chain fatty acids in health and disease. *Adv Immunol*. 2014;121:91–119. doi:10.1016/b978-0-12-800100-4.00003-9
24. Tomoda K, Kubo K, Dairiki K, et al. Whey peptide-based enteral diet attenuated elastase-induced emphysema with increase in short chain fatty acids in mice. *BMC Pulm Med*. 2015;15(1):64. doi:10.1186/s12890-015-0059-2
25. Parada Venegas D, De LA Fuente MK, Landskron G, et al. Short Chain Fatty Acids (SCFAs)-Mediated Gut Epithelial and Immune Regulation and Its Relevance for Inflammatory Bowel Diseases. *Front Immunol*. 2019;10:277. doi:10.3389/fimmu.2019.00277
26. Corrêa-Oliveira R, Fachi JL, Vieira A, Sato FT, Vinolo MA. Regulation of immune cell function by short-chain fatty acids. *Clin Transl Immunol*. 2016;5(4):e73. doi:10.1038/cti.2016.17
27. den Besten G, van Eunen K, Groen AK, Venema K, Reijngoud DJ, Bakker BM. The role of short-chain fatty acids in the interplay between diet, gut microbiota, and host energy metabolism. *J Lipid Res*. 2013;54(9):2325–2340. doi:10.1194/jlr.R036012
28. Canani RB, Costanzo MD, Leone L, Pedata M, Meli R, Calignano A. Potential beneficial effects of butyrate in intestinal and extraintestinal diseases. *World J Gastroenterol*. 2011;17(12):1519–1528. doi:10.3748/wjg.v17.i12.1519
29. Inan MS, Rasoulpour RJ, Yin L, Hubbard AK, Rosenberg DW, Giardina C. The luminal short-chain fatty acid butyrate modulates NF-kappaB activity in a human colonic epithelial cell line. *Gastroenterology*. 2000;118(4):724–734. doi:10.1016/s0016-5085(00)70142-9
30. Li N, Liu XX, Hong M, et al. Sodium butyrate alleviates LPS-induced acute lung injury in mice via inhibiting HMGB1 release. *Int Immunopharmacol*. 2018;56:242–248. doi:10.1016/j.intimp.2018.01.017
31. Vendrik KEW, Ooijevaar RE, de Jong PRC, et al. Fecal Microbiota Transplantation in Neurological Disorders. *Front Cell Infect Microbiol*. 2020;10:98. doi:10.3389/fcimb.2020.00098
32. Jang YO, Lee SH, Choi JJ, et al. Fecal microbial transplantation and a high fiber diet attenuates emphysema development by suppressing inflammation and apoptosis. *Exp Mol Med*. 2020;52(7):1128–1139. doi:10.1038/s12276-020-0469-y

33. den Besten G, van Eunen K, Groen AK, et al. The role of short-chain fatty acids in the interplay between diet, gut microbiota, and host energy metabolismThe role of short-chain fatty acids in the interplay between diet, gut microbiota, and host energy metabolism. *J Lipid Res*. 2013;54 (9):2325–40. doi:10.1194/jlr.R036012
34. Canani RB, Costanzo MD, Leone L, et al. Potential beneficial effects of butyrate in intestinal and extraintestinal diseases. *World J Gastroenterol*. 2011;17(12):1519–28. doi:10.3748/wjg.v17.i12.1519
35. Inan MS, Rasoulpour RJ, Yin L, et al. The luminal short-chain fatty acid butyrate modulates NF-kappaB activity in a human colonic epithelial cell line. *Gastroenterology*. 2000;118(4):724–34. doi:10.1016/s0016-5085(00)70142-9
36. Li N, Liu XX, Hong M, et al. Sodium butyrate alleviates LPS-induced acute lung injury in mice via inhibiting HMGB1 release. *Int Immunopharmacol*. 2018;56:242–248. doi:10.1016/j.intimp.2018.01.017
37. Vendrik KEW, Ooijevaar RE, de Jong PRC, et al. Fecal Microbiota Transplantation in Neurological Disorders. Front Cell Infect Microbiol.. *Exp Mol Med*. 2020;52(7):1128–1139. doi:10.3389/fcimb.2020.00098
38. Jang YO, Lee SH, Choi JJ, et al. Fecal microbial transplantation and a high fiber diet attenuates emphysema development by suppressing inflammation and apoptosis. *Exp Mol Med*. 2020;52(7):1128–1139. doi:10.1038/s12276-020-0469-y